frontiers | Frontiers in Electronic Materials

ORIGINAL RESEARCH
published: 07 April 2022
doi: 10.3389/femat.2022.861448

Electronic Tuning in URu_2Si_2 Through Ru to Pt Chemical Substitution

Greta L. Chappell[1,2], *William L. Nelson*[1,2], *D. E. Graf*[1] *and Ryan E. Baumbach*[1,2]*

[1]National High Magnetic Field Laboratory, Florida State University, Tallahassee, FL, United States, [2]Department of Physics, Florida State University, Tallahassee, FL, United States

Studies that control the unit cell volume and electronic composition have been useful in revealing what factors lead to hidden order and superconductivity in the strongly correlated electron system URu_2Si_2. For example, isoelectronic tuning that increases the hybridization between the *f* and conduction electron states (i.e., applied pressure and Ru → Fe/Os chemical substitution) 1) converts hidden order into antiferromagnetism and 2) destroys the superconductivity. The impact of nonisoelectronic chemical substitution has been less clear, but several unifying trends have recently emerged for chemical substitution vectors that qualitatively add electrons (e.g., Ru → Rh/Ir and Si → P). This includes 1) the rapid destruction of hidden order and superconductivity, 2) composition regions where the underlying Kondo lattice is preserved but does not harbor an ordered state, and 3) the emergence of complex magnetism at large substitutions. In order to assess the limits of this perspective, we have investigated the series $U(Ru_{1-x}Pt_x)_2Si_2$ for $x \lesssim 0.19$, where the Ru and Pt *d*-shells differ substantially from each other. Magnetic susceptibility, electrical resistivity, and heat capacity measurements unexpectedly reveal a phase diagram with notable similarities to those of other electron doping series. This result reinforces the viewpoint that there is a quasi-universal affect that results from electron doping in this material, and we anticipate that an understanding of these trends will be useful to isolate what factors are foundational for hidden order and superconductivity.

Keywords: hidden order in URu_2Si_2, unconventional superconducivity, Kondo lattice and heavy fermions, chemical substitution, magnetism

OPEN ACCESS

Edited by:
Vidya Madhavan, University of Illinois at Urbana-Champaign, United States

Reviewed by:
John Tranquada, Brookhaven National Laboratory (DOE), United States
Huixia Luo, Sun Yat-sen University, China

***Correspondence:**
Ryan E. Baumbach
baumbach@magnet.fsu.edu

Specialty section:
This article was submitted to Superconducting Materials, a section of the journal Frontiers in Electronic Materials

Received: *24 January 2022*
Accepted: *07 March 2022*
Published: *07 April 2022*

Citation:
Chappell GL, Nelson WL, Graf DE and Baumbach RE (2022) Electronic Tuning in URu_2Si_2 Through Ru to Pt Chemical Substitution. Front. Electron. Mater. 2:861448. doi: 10.3389/femat.2022.861448

1 INTRODUCTION

The heavy fermion superconductor (T_c = 1.4 K) URu_2Si_2 has attracted sustained interest since its discovery in 1985, owing mainly to the enigmatic hidden order (HO) phase that it enters through a second-order phase transition at T_0 = 17.5 K (Palstra et al., 1985; Maple et al., 1986; Schlabitz et al., 1986). Like many of the related UT_2X_2 (*T* = transition metal and *X* = Si, Ge) compounds (Żołnierek and Mulak, 1995), URu_2Si_2 crystallizes in the ubiquitous $ThCr_2Si_2$-type tetragonal structure and exhibits Kondo-lattice hybridization of the *f* electrons with the conduction electrons (Endstra et al., 1993). However, in contrast to these chemical/structural analogs, many of which exhibit more conventional low-temperature behavior (e.g., antiferromagnetism in URh_2Si_2 (Umarji et al., 1987) and Pauli paramagnetism in UFe_2Si_2 (Szytuka et al., 1988)), extensive investigations have not yet led to a definitive understanding of hidden order, why it is able to host superconductivity, and what factors are key in promoting its unique behavior.

A productive strategy for addressing these questions has been to perturb the electronic state and structure using tuning parameters such as applied pressure (McElfresh et al., 1987; Motoyama et al.,

2003; Hassinger et al., 2008; Butch et al., 2010), magnetic fields (De Boer et al., 1986; Nieuwenhuys, 1987; Kim et al., 2003a; Kim et al., 2003b), and chemical substitution (Amitsuka et al., 1988; Dalichaouch et al., 1989; Dalichaouch et al., 1990a; Dalichaouch et al., 1990b; Miyako et al., 1991; Kawarazaki et al., 1994; Yokoyama et al., 2004; Bauer et al., 2005; Jeffries et al., 2007; Yokoyama and Amitsuka, 2007; Butch and Maple, 2009; Butch and Maple, 2010; Kanchanavatee et al., 2011; Kanchanavatee et al., 2014; Das et al., 2015; Ran et al., 2016; Wilson et al., 2016). Applied pressure (McElfresh et al., 1987; Motoyama et al., 2003; Hassinger et al., 2008; Butch et al., 2010) and isoelectronic chemical substitution at the Ru site [Ru → Fe, Os (Kanchanavatee et al., 2011; Kanchanavatee et al., 2014; Das et al., 2015; Ran et al., 2016; Wilson et al., 2016)] produce similar results: as the hybridization strength increases, HO is first enhanced, and then it is converted to antiferromagnetism (LMAFM). Superconductivity is only observed within the HO region. Nonisoelectronic substitution at the Ru site is less straightforward: Ru → Mn, Tc, Re substitution (Dalichaouch et al., 1989; Dalichaouch et al., 1990a; Dalichaouch et al., 1990b; Bauer et al., 2005; Jeffries et al., 2007; Butch and Maple, 2009; Butch and Maple, 2010) (effectively removing electrons) suppresses HO and stabilizes complex ferromagnetism, while Ru → Rh, Ir (Amitsuka et al., 1988; Dalichaouch et al., 1990a; Miyako et al., 1991; Kawarazaki et al., 1994; Yokoyama et al., 2004; Yokoyama and Amitsuka, 2007) (effectively adding electrons) suppresses HO, stabilizes a region with no long range magnetic order, and eventually gives rise to a new antiferromagnetically ordered state. More recently, studies have shown that Si → P substitution produces a similar phase diagram (Gallagher et al., 2016a; Gallagher et al., 2016b; Chappell et al., 2020). This raises the possibility that nonisoelectronic chemical substitution that effectively adds electrons, regardless of how it is accomplished, may result in a unified phase diagram. This is unexpected given the differences between 1) substitution at the Ru or Si sites, which are crystallographically distinct, and 2) differences between substitution of 3*d*, 4*d*, 5*d*, and *s*/*p* electrons, which have differing valence-electron wave functions and may impact hybridization in different ways.

In order to probe the possibility that some nonisoelectronic substitution series share related phase diagrams, we investigated the chemical substitution series $U(Ru_{1-x}Pt_x)_2Si_2$. Here, Ru → Pt substitution is expected to be distinct from earlier electron doping series because 1) Ru is a 4*d* element while Pt is a 5*d* element, 2) Ru → Rh and Si → P are adjacent periodic table column substitutions while Ru → Pt is not, and 3) distinct bonding occurs for UPt_2Si_2 (Ptasiewicz-Bąk et al., 1985; Lee et al., 2018; Lee et al., 2020), as evidenced by its formation in the $CaBe_2Ge_2$ structure. These differences might be expected to drive the appearance of a distinct T–x phase diagram, as suggested by studies of other families of materials where transition metal → Pt substitution has been shown to be a versatile tuning parameter. (Zhu et al., 2010; Luo et al., 2013). Instead of this, temperature-dependent magnetic susceptibility, electrical resistivity, heat capacity, and high-field magnetoresistivity measurements reveal striking similarities to earlier reported phase diagrams in which tuning effectively adds electrons (Amitsuka et al., 1988; Dalichaouch et al., 1990a; Miyako et al., 1991; Kawarazaki et al., 1994; Yokoyama et al., 2004; Yokoyama and Amitsuka, 2007; Gallagher et al., 2016a; Gallagher et al., 2016b). In particular, the HO phase boundary is rapidly suppressed and abruptly collapses before $x \approx 0.03$. Superconductivity is only observed for the parent compound, which may suggest that HO is rapidly converted to AFM by $x \approx 0.02$. This is followed by a region ($0.03 \lesssim x \lesssim 0.05$) with a paramagnetic (PM) Kondo lattice with a heavy-Fermi-liquid ground state and no ordering is seen down to low temperatures. Finally, magnetic order with an antiferromagnetic character emerges and strengthens for $0.06 \lesssim x \lesssim 0.19$, although it is distinct from what is seen for other tuning series (Amitsuka et al., 1988; Dalichaouch et al., 1990a; Miyako et al., 1991; Kawarazaki et al., 1994; Yokoyama et al., 2004; Yokoyama and Amitsuka, 2007; Gallagher et al., 2016a; Gallagher et al., 2016b; Rahn et al., 2021). These results provide evidence that although Ru → Pt, Rh and Si → P chemical substitutions are each distinct in their own way, they nonetheless provide semiunified tuning in URu_2Si_2 that is likely connected to charge doping.

2 EXPERIMENTAL METHODS

Polycrystalline samples of $U(Ru_{1-x}Pt_x)_2Si_2$ were synthesized by arc melting elements (99.99+% pure, lump form) in a 1:(2–2x):2x:2 M ratio of U:Ru:Pt:Si. The chemical composition and x values were determined using electron-dispersive spectroscopy (EDS) by averaging the measured values taken from multiple areas within specimens (see **Supplementary Figure S1**). For nominal concentrations $x_{nom} \leq 0.05$, the measured $x_{meas} \approx x_{nom}$ and there is little variation across the samples. For $0.075 \leq x_{\{nom\}} \leq 0.12$, $x_{meas} < x_{nom}$, but there is little variation across the samples. Finally, for $x_{nom} = 0.15$ there is substantial variation across the sample, suggesting that this is near the limit for uniform Pt substitution and above this value chemical separation may be present. Throughout the rest of the manuscript $x = x_{meas,\ avg}$, as defined in **Supplementary Figure S1**. The crystal structure (see **Supplementary Figure S2**) was verified by powder x-ray diffraction spectroscopy (pXRD) using a Scintag diffractometer with a copper source. The a and c lattice constants were extracted from the data using Rietveld refinement with WinPrep90 software.

Magnetization measurements were done using a Quantum Design Magnetic Property Measurement System in an applied magnetic field $H = 5$ kOe and at temperatures $T = 1.8$–300 K. The samples that were used for these measurements were crushed into powder in order to measure the polycrystalline average magnetic susceptibility $\chi_{avg} = (\chi_c + 2\chi_{ab})/3$. Electrical resistivity $\rho(T)$ measurements were done using a standard four-wire resistance probe in a Quantum Design Physical Property Measurement System (PPMS) at temperatures $T = 1.8$–300 K using a He4 cryostat and also for $T = 0.14$–20 K with an adiabatic demagnetization refrigerator PPMS insert. Heat capacity measurements were conducted using the thermal relaxation method in a PPMS for $T = 1.8$–55 K. Magnetoresistivity measurements were carried out for semi-aligned large grain

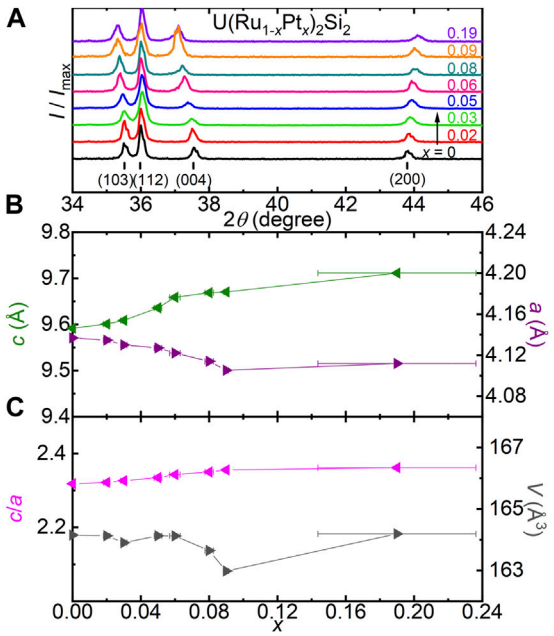

FIGURE 1 | (A) The powder x-ray diffraction intensity normalized to the maximum value I/I_{max} vs. scattering angle 2θ for $U(Ru_{1-x}Pt_x)_2Si_2$ $x \lesssim 0.19$ (patterns are vertically shifted for clarity) zoomed in on the peaks displaying strong shifting with increases x. Black vertical bars denote the peak centers corresponding to the (*hkl*) crystallographic planes for URu_2Si_2 that are listed near the bottom axis. **(B)** The c (left axis) and a (right axis) lattice constants vs. x determined by Rietveld refinement of the powder patterns. **(C)** Lattice constants ratio c/a (left axis) and unit cell volume V (right axis) vs. x.

specimens using a resistive magnet at the NHMFL facility in Tallahassee FL at $T \approx 0.39$ K and with the applied field $H \leq 41$ T parallel to the crystallographic c axis.

3 RESULTS

The powder x-ray diffraction patterns for $U(Ru_{1-x}Pt_x)_2Si_2$ (**Figure 1A**; **Supplementary Figure S2**) show that for $x \lesssim 0.19$ specimens crystallize in the $ThCr_2Si_2$ structure and do not exhibit impurity peaks, even for the concentration $x \approx 0.19$ that has a large distribution in the Pt chemical composition determined by EDS. **Figure 1A** focuses on several peaks that are associated with principal crystallographic directions, where the (004) and (200) peaks noticeably shift in opposite directions with increasing x. This indicates that the substitution of Pt has distinct influences on the in plane and out of plane bonding, and Rietveld refinement of the data shows that the c and a values increase and decrease, respectively, with increasing x. Furthermore, the calculated unit cell volume V and lattice parameter ratio c/a (**Figure 1C**) remain nearly constant for all x. Taken together, these trends suggests that Ru → *Pt* substitution is analogous to a negative uniaxial pressure that expands the c axis and compresses the ab plane, although the influence of nonisoelectronic chemical substitution cannot be neglected (discussed below). The exception is that the lattice constant a deviates from the low-x trend for $x \approx 0.19$, which may be related to chemical inhomogeneity that was observed in chemical analysis measurements.

Results for the polycrystalline average magnetic susceptibility $\chi_{avg}(T) = (\chi_c + 2\chi_{ab})/3$ are shown in **Figure 2**. The curve for $x = 0$ shows the expected Curie-Weiss behavior at elevated temperatures, a Kondo coherence maximum at $T_{coh,\chi_{avg}} \approx 55$ K, and a kink at the HO transition at $T_0 \approx 17.4$ K (Palstra et al., 1985; Maple et al., 1986; Schlabitz et al., 1986; Baumbach et al., 2014). The high temperature behavior is unchanged for all x, but there is a distinct evolution for low temperatures. In particular, 1) T_0 shifts to lower temperature for $x \approx 0.02$, 2) it is removed for $x \approx 0.03$–0.05 (suggesting that there is no ordered state over this x range), and 3) for $x \approx 0.06$–0.19 there is a strong reduction in $\chi_{avg}(T)$ that is consistent with the onset of antiferromagnetic ordering at T_N. This feature is emphasized in the derivative of the data (**Figure 2B**), where T_N is defined as the midpoint of the upturn in $d\chi_{avg}/dT$ (downward-facing triangles) and the bars indicate the width in temperature of the transitions. This yields an ordering temperature $T_N \approx 42$ K for $x = 0.19$ and, although it weakens with decreasing x, the ordering potentially extends as low as $x \approx 0.06$ where T_N is slightly suppressed. The electrical transport and heat capacity measurements shown below support this perspective. Interestingly, hysteresis is also seen at large x for $T < T_N$ and appears to strengthen with increasing x. This suggests that, while this ordered state has an antiferromagnetic character, it likely hosts additional complexity. In order to resolve this question, an investigation of the magnetic anisotropy for single-crystal specimens or neutron-scattering measurements will be necessary.

Temperature-dependent electrical resistivity $\rho/\rho_{300K}(T)$ results are shown in **Figure 3**. The expected behavior is seen for $x = 0$ (Maple et al., 1986; Schlabitz et al., 1986;

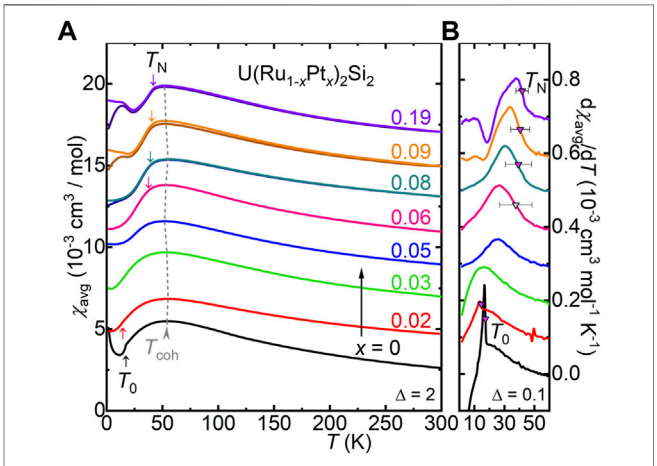

FIGURE 2 | (A) Polycrystalline average magnetic susceptibility $\chi_{avg} = (\chi_c + 2\chi_{ab})/3$ vs. temperature T for $U(Ru_{1-x}Pt_x)_2Si_2$ $x \lesssim 0.19$. The temperature at the maximum in χ_{avg}, T_{coh}, is indicated by the vertical-dashed line. **(B)** Derivative of the polycrystalline average magnetic susceptibility with respect T, $d\chi_{avg}/dT$, vs. T zoomed in on the phase transitions. Phase transition temperatures are indicated with colored arrows in **(A)** and downward-facing triangles in **(B)**. Bars indicate the width in temperature of the transitions. Curves are vertically shifted by Δ for clarity.

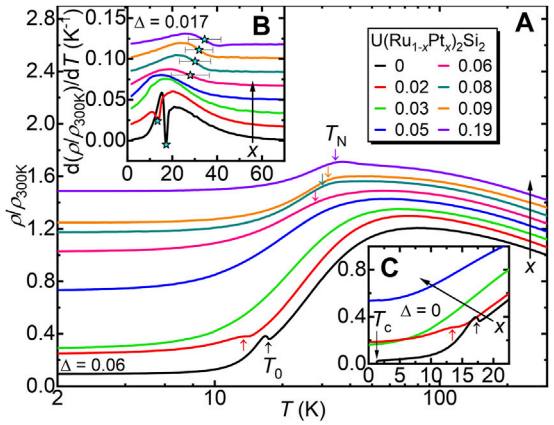

FIGURE 3 | (A) The electrical resistivity normalized to the room temperature value ρ/ρ_{300K} vs. log(T) for $U(Ru_{1-x}Pt_x)_2Si_2$ $x \lesssim 0.19$. **(B)** The derivative of ρ/ρ_{300K} with respect to T, $d(\rho/\rho_{300K})/dT$, vs. T zoomed in on the HO and AFM phase transitions. **(C)** ρ/ρ_{300K} vs. T for $x \lesssim 0.05$ and $T \gtrsim$ 140 mK zoomed in on the SC and HO phase transitions. The curves are vertically offset by Δ for clarity. The phase transition temperatures are indicated with arrows in **(A,C)** and star symbols in **(B)**, where the bars indicate the widths.

Baumbach et al., 2014; Palstra et al., 1986), where $\rho/\rho_{300K}(T)$ first increases with decreasing temperature and subsequently goes through a maximum near $T_{coh,\rho} \approx 75$ K as the coherent Kondo lattice forms. Similar behavior persists for $x \lesssim 0.05$, where there is little change in $T_{coh,\rho}$. As is seen in $\chi_{avg}(T)$, the HO transition (defined as the local minimum in $d(\rho/\rho_{300K})/dT$, **Figure 3B**) shifts to lower T for $x \approx 0.02$ and is not present for larger concentrations. Although $x \approx 0.02$ exhibits ordering that connects to the hidden order phase boundary, measurements as low as 280 mK reveal no evidence for superconductivity (SC) (**Figure 3C**, inset). This is distinct from what is seen in other substitution series (e.g., Si → P (Gallagher et al., 2016a; Gallagher et al., 2016b) and Ru → Fe (Kanchanavatee et al., 2011)), where hidden order hosts SC even for chemically substituted specimens. The reason for the absence of SC is not clear, but it may suggest that, instead of enabling a smooth suppression of hidden order, Pt substitution stabilizes a magnetic phase that is similar to the antiferromagnetism that is seen at low x in the Ru → Rh series (Dalichaouch et al., 1990a; Amitsuka et al., 1988; Miyako et al., 1991; Kawarazaki et al., 1994; Yokoyama et al., 2004; Yokoyama and Amitsuka, 2007) or the parasitic small moment antiferromagnetism that occurs due to defects in the parent compound (Niklowitz et al., 2010). Recent results also suggest that antiferromagnetism intervenes in the Si → P substitution series at the boundary of the hidden order phase (Chappell et al., 2020). Once the low-x ordering is suppressed, there is no evidence for an ordered state for $x \approx 0.03$–0.05 at temperatures above 140 mK. In $\rho/\rho_{300K}(T)$ at large x, the antiferromagnetic ordering appears as a subtle humplike feature that is followed by a reduction of the resistivity at low temperatures. These features are more evident in the derivative of the data (**Figure 3B**), and this characteristic shape is observed for $x \gtrsim 0.06$. The transition temperature, defined as the midpoint of the upturn in $d(\rho/\rho_{300K})/dT$ (star symbols and bars to indicate the temperature widths, **Figure 3B**), shifts to slightly higher temperature with increasing x and is in agreement with the values of T_N that are seen in $\chi_{avg}(T)$. Also noteworthy is that the shape of the anomaly in $\rho/\rho_{300K}(T)$ evolves, becoming gradually more humplike at larger x. This could indicate that a change in the magnetic ordering is taking place. Over the large-x range, $T_{coh,\rho}$ is difficult to define, because it occurs at temperatures that are similar to that of the magnetic ordering; however, it appears to roughly remain constant. Finally, we note that the residual resistivity increases strongly with increasing x. This may be due to disorder effects, but note that over similar x ranges in other substitution series (e.g., $URu_{2-x}Rh_xSi_2$ (Dalichaouch et al., 1990a), $URu_{2-x}(Fe,Os)_xSi_2$ (Kanchanavatee et al., 2011; Kanchanavatee et al., 2014), and $URu_2Si_{2-x}P_x$ (Gallagher et al., 2016a; Gallagher et al., 2016b)) this effect is much weaker. Therefore, we speculate that this could instead be associated with an intrinsic electronic effect.

The heat capacity results are shown in **Figure 4** and **Supplementary Figure S4**. The peak that is associated with the HO transition decreases for $x \approx 0.02$ and is removed for $x \approx 0.03$ (**Figure 4A**). Similar to the Si → P (Gallagher et al., 2016a; Gallagher et al., 2016b) and Ru → Rh (Amitsuka et al., 1988) substitution series, the height of the peak decreases and the low temperature value of C/T increases over this x region. In the region $x \approx 0.03$–0.05, there is no evidence for an ordered state,

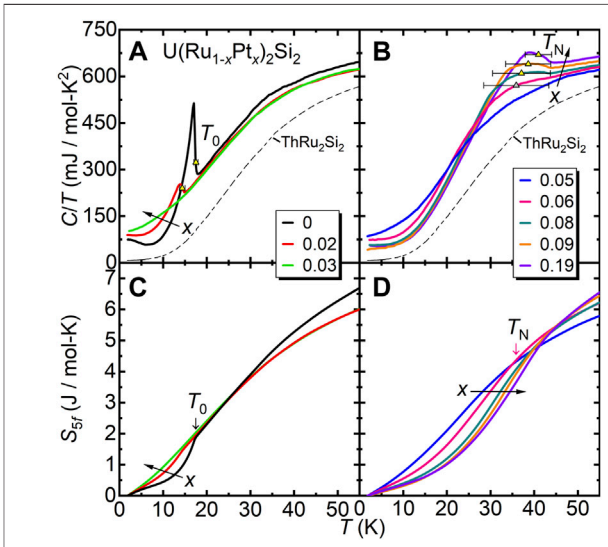

FIGURE 4 | The heat capacity divided by temperature C/T vs. T for $U(Ru_{1-x}Pt_x)_2Si_2$ **(A)** $x = 0$, $x \approx 0.02$, $x \approx 0.03$, and **(B)** $x \approx 0.05$, $x \approx 0.06$, $x \approx 0.08$, $x \approx 0.09$, $x \approx 0.19$. The ordering temperatures T_0 and T_N are indicated by open squares and triangles, respectively. The dashed curve is for $ThRu_2Si_2$, a nonmagnetic analog of URu_2Si_2. **(C,D)** The 5f orbital magnetic entropy S_{5f} vs. T of the data in **(A,B)**, respectively, that is calculated as described in the text. Plots of the 5f contribution to the heat capacity are shown in **Supplementary Figure S4**.

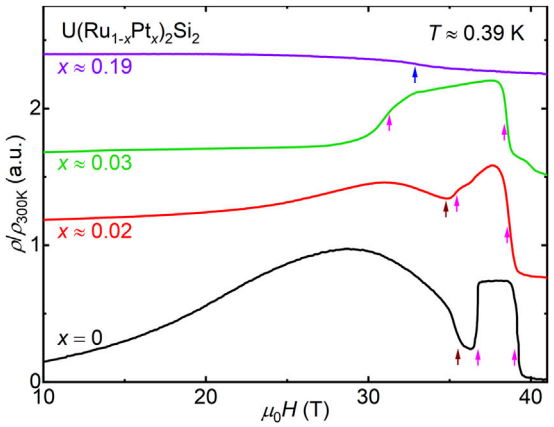

FIGURE 5 | The magnetoresistivity normalized to the room temperature value ρ/ρ_{300K} vs. applied magnetic field $\mu_0 H$ for $U(Ru_{1-x}Pt_x)_2Si_2$ x = 0, 0.02, 0.03, 0.19 (curves are vertically offset for clarity). The red arrow indicates the hidden order phase transition, the magenta arrows indicate the field-induced phase, and the blue arrow indicates the AFM transition.

but Fermi-liquid behavior is observed where the electronic component γ remains enhanced. The AFM transition for $x \approx 0.06$ (**Figure 4B**) develops from a broad peak to a more pronounced peak for $x \approx 0.19$ and is similar to the AFM transition seen in the phosphorus-substituted series (Gallagher et al., 2016a; Gallagher et al., 2016b). T_N is taken as the midpoint of the local minimum and maximum, and the bars indicate the temperature widths of the transitions. We also note that for specimens that exhibit antiferromagnetism, the low-temperature value of C/T is reduced from what is seen at lower x.

In **Figures 4C,D**, the magnetic entropy S_{5f} is shown, which is calculated by subtracting C/T of the nonmagnetic analog $ThRu_2Si_2$ (gray-dashed curve) and integrating from 1.8 − 55 K. As seen earlier for the Si → P series (Gallagher et al., 2016a; Gallagher et al., 2016b), the entropy associated with the HO transition is reduced for the chemically substituted sample. For samples with AFM, S_{5f} gradually increases overall, and the reduction following T_N is consistent with the loss of entropy due to the magnetic ordering. The behavior of $S_{5f}(T)$ and its value at T_N is comparable to what is seen for the Si → P series at large x.

Finally, results for electrical resistivity measurements under applied magnetic fields are shown in **Figure 5**. The behavior for $x = 0$ is well known (De Boer et al., 1986; Nieuwenhuys, 1987; Kim et al., 2003a; Kim et al., 2003b), where a complex family of high-field ordered states was previously described. For $x \approx 0.02$, the curve is reminiscent of what is seen for the parent compound: there is initially a strong increase and broad peak around 31 T that is abruptly followed by a cascade of transitions, and an eventual strong reduction in the resistivity near 38 T when the system enters the high-field polarized phase. The behavior for $x \approx 0.03$ is distinct from what is seen in the HO x region. Here, the initial increase in ρ/ρ_{300K} is weak and there is an abrupt increase near 31 T that is followed by an abrupt decrease at 38 T. This square shape curve is reminiscent of what was previously seen in Si → P (Wartenbe et al., 2017; Huang et al., 2019) and Ru → Rh (Kuwahara et al., 2013) substitution series within the x range that hosts a paramagnetic Kondo lattice without long-range ordered ground states. Finally, for $x \approx 0.19$, ρ/ρ_{300K} decreases weakly with H until it undergoes a more rapid reduction near 33 T, indicating the occurrence of a metamagnetic phase transition. This is similar to what was earlier seen in the antiferromagnetic x region for the Si → P series (Wartenbe et al., 2017; Huang et al., 2019), although the critical field is substantially reduced.

4 DISCUSSION

The phase diagram for $U(Ru_{1-x}Pt_x)_2Si_2$ $x \lesssim 0.19$, constructed from $\chi_{avg}(T)$, $\rho/\rho_{300K}(T)$, and $C/T(T)$ is shown in **Figure 6**. The HO transition is suppressed for $x \lesssim 0.02$ and abruptly collapses before $x \approx 0.03$ (red shaded region). Superconductivity is only observed for the parent compound, which may suggest that hidden order is rapidly converted to antiferromagnetism, similar to what is seen in the Ru → Rh substitution series (Dalichaouch et al., 1990a; Amitsuka et al., 1988; Miyako et al., 1991; Kawarazaki et al., 1994; Yokoyama et al., 2004; Yokoyama and Amitsuka, 2007) and under applied pressure (McElfresh et al., 1987; Motoyama et al., 2003; Hassinger et al., 2008; Butch et al., 2010; Niklowitz et al., 2010). This is followed by a region ($0.03 \lesssim x \lesssim 0.05$) with a paramagnetic (PM) Kondo lattice with a heavy-Fermi-liquid ground state that is similar to the high-temperature behavior for $x = 0$, but no ordering is seen down to low temperatures (arrows). Finally, magnetic order with an antiferromagnetic character emerges and strengthens for $0.06 \lesssim x \lesssim 0.19$ (blue shaded region). The data for $x \approx 0.06$ are highlighted in gray because the phase

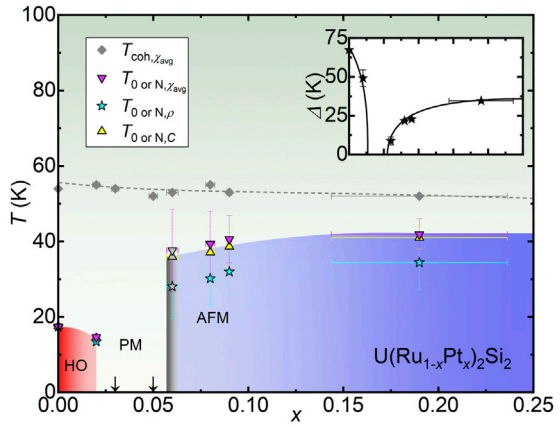

FIGURE 6 | The transition temperature T vs. x phase diagram for $U(Ru_{1-x}Pt_x)_2Si_2$ $x \lesssim 0.19$ constructed from measurements of polycrystalline average magnetic susceptibility χ_{avg} (down-facing triangles), electrical resistivity ρ/ρ_{300K} (stars), and heat capacity C (up-facing triangles). The coherence temperatures T_{coh} from χ_{avg} are the square symbols and the dashed gray line is a guide for the eyes. Inset: Energy gap Δ from fits to ρ/ρ_{300K} data as described in the text.

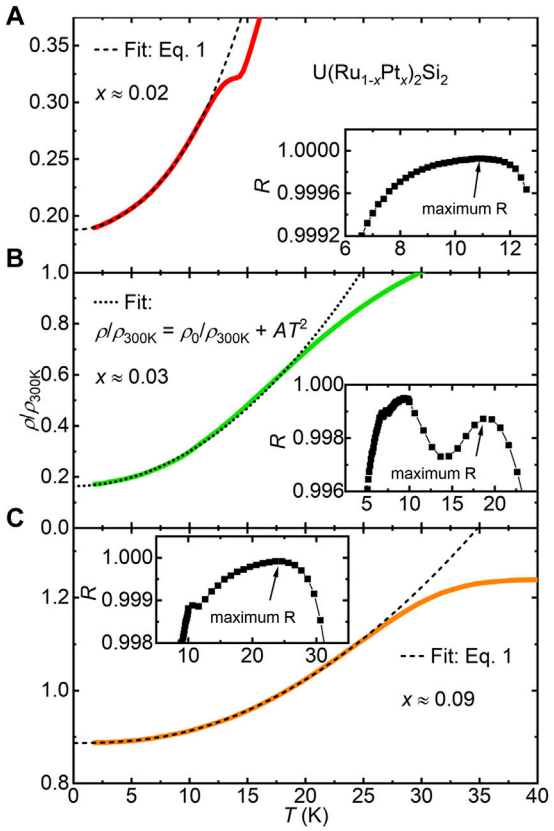

FIGURE 7 | ρ/ρ_{300K} vs. T for $U(Ru_{1-x}Pt_x)_2Si_2$ $x \approx$ **(A)** 0.02, **(B)** 0.03, and **(C)** 0.09. The dashed and dotted lines are the best fits to the data as described in the text. Insets: Goodness of fit R vs. the maximum temperature of the fit range T_{max}.

transition is difficult to detect and is only distinguished in the heat capacity measurement. Also noteworthy is that there is an evolution in the large-x magnetic behavior, which is characterized by the appearance of hysteresis in $\chi_{avg}(T)$ and a change in the shape of the $\rho/\rho_{300K}(T)$ curve. Finally, the Kondo coherence temperature T_{coh} in $\chi_{avg}(T)$ (dashed gray line in **Figures 2A**, **6**) appears to remain constant, or slightly decreases with increasing x, suggesting that the Kondo lattice itself is nearly insensitive to doping. Taken together, these results reveal a strong similarity between the Ru → Pt phase diagram and those for the Ru → Rh (Amitsuka et al., 1988; Dalichaouch et al., 1990a; Miyako et al., 1991; Kawarazaki et al., 1994; Yokoyama et al., 2004; Yokoyama and Amitsuka, 2007) and Si → P (Gallagher et al., 2016a; Gallagher et al., 2016b) substitution series, all of which feature an evolution from the HO to NO to AFM regions with increasing x and a robust Kondo-lattice energy scale that is somewhat insensitive to chemical substitution. Furthermore, the evolution of the field induced phases in the various regions resembles earlier results in other series. These similarities are unexpected, given that in each case 1) the lattice tuning is distinct and 2) the type of electrons that are being added differ substantially from each other. By clarifying the reasons for this similarity, it may be possible to further understand the factors that lead to the stability of hidden order in this distinct region of the electronic phase space. One attempt to do this was recently seen for the Si → P series, where tight-binding Hartree-Fock calculations show 1) that the radial probability distributions for the phosphorus ions are more tightly bound than that of the silicon and 2) that the energy difference between the orbitals decreases with increasing x (Chappell et al., 2020). The cumulative effect is that Si → P substitution decreases the hybridization strength, which correlates with the weakening of HO. At larger x, electrical charge tuning has been proposed to play an important role in determining the ground-state behavior. From this perspective, it might be proposed that Ru → Rh and Pt substitution also evolve along similar tuning axes, where decreasing hybridization strength and addition of charge carriers simultaneously tune the behavior. We note that this scenario is supported by earlier work studying trends in the UT_2X_2 (T = transition metal and X = Si,Ge) family, which suggest that the hybridization strength tends to decrease going from the Fe column towards the Cu column. Furthermore, all examples in the Co, Ni, and Cu columns exhibit magnetic ordering due to the uranium ions. (Endstra et al., 1993).

Finally, in order to gain further insight into the different regions of the phase diagram, fits to the low-temperature-normalized resistivity were done using the expression,

$$\rho \Big/ \rho_{300K}(T) = \rho_0 \Big/ \rho_{300K} + AT^2 + B\frac{T}{\Delta}\left(1 + \frac{T}{\Delta}\right)e^{-\Delta/T} \qquad (1)$$

where ρ_0/ρ_{300K} is the normalized residual resistivity, AT^2 is the Fermi-liquid term, and the final term represents electron-magnon scattering due to spin excitations with an energy gap Δ (**Figure 7**) (McElfresh et al., 1987; Hassinger et al., 2008; Chappell et al., 2020; Palstra et al., 1986; Jeffries et al., 2008; Motoyama et al., 2008). It is already established that this expression merely provides a phenomenological description of the data and does not suggest that the hidden ordering is due to simple magnetism. We nonetheless use it in order to make a direct comparison to earlier studies, where Δ is associated with an energy gap that opens over the Fermi surface; e.g., as seen in measurements such as the heat capacity (Maple et al., 1986), inelastic neutron scattering (Wiebe et al., 2007), and angle-resolved photo-emission spectroscopy (ARPES) (Santander-Syro et al., 2009; Yoshida et al., 2010; Meng et al., 2013; Bareille et al., 2014). The best fits to the data were determined by varying the maximum temperature of the fit range T_{max}, and evaluating the maximum of the goodness of the fits R. For concentrations exhibiting HO ($x \lesssim 0.02$) or AFM ($0.06 \lesssim x \lesssim 0.19$) the maximum in R is greater than 0.999. For concentrations with no ordering ($0.03 \lesssim x \lesssim 0.05$) fits to the data using **Eq. 1** yielded $\Delta = 0$ (**Figure 7B**). Results for the energy gap Δ are shown in the inset of **Figure 6**, where Δ decreases with increasing x in the HO region, mirroring the HO phase boundary. In the AFM x-region, Δ grows with increasing x and saturates near 35 K. These trends are similar to what was earlier seen for Si → P, where Δ

decreases from 70 to 40 K in the HO region (Gallagher et al., 2016a; Gallagher et al., 2016b; Chappell et al., 2020). However, the absolute value of Δ differs from what was seen for the Si → P series, where Δ saturates at a larger value near 100 K. This provides some evidence that this type of magnetic ordering is distinct from that seen in other tuning series.

5 CONCLUSION

We have introduced the phase diagram for $U(Ru_{1-x}Pt_x)_2Si_2$ $x \lesssim 0.19$ constructed from $\chi(T)$, $\rho(T)$, and $C(T)$ measurements. The HO transition is suppressed and abruptly collapses before $x \approx 0.03$. Superconductivity is only observed for the parent compound, which may suggest that HO is rapidly converted to magnetic order by $x \approx 0.02$. For $0.03 \lesssim x \lesssim 0.05$, no ordering is observed for $T \gtrsim 280$ mK and there is a PM Kondo lattice with a heavy-Fermi-liquid ground state. For $0.06 \lesssim x \lesssim 0.19$, magnetic order with an antiferromagnetic character and hysteresis for $T < T_N$ emerges and strengthens with increasing x. The similarity of this phase diagram with those of the Si → P (Gallagher et al., 2016a; Gallagher et al., 2016b) and Ru → Rh (Amitsuka et al., 1988; Dalichaouch et al., 1990a; Miyako et al., 1991; Kawarazaki et al., 1994; Yokoyama et al., 2004; Yokoyama and Amitsuka, 2007) chemical substitution series is noteworthy. To explain this, we suggest that their phase diagrams are controlled by a semi-universal combination of weakening hybridization strength and electron substitution. In order to fully understand this series, it will be useful to investigate single-crystal specimens of this series in order to determine the anisotropy in $\rho(T)$ and $\chi(T)$, and to carry out more detailed studies of the Fermi surface and magnetic ordering in order to make comparisons to the P and Rh doped compounds.

DATA AVAILABILITY STATEMENT

The raw data supporting the conclusion of this article will be made available by the authors, without undue reservation.

AUTHOR CONTRIBUTIONS

RB designed the project, supervised its completion, contributed to data analysis and wrote the manuscript. GC synthesized the specimens, carried out measurements, contributed to data analysis and wrote the manuscript. WN contributed to synthesis and experiments. DG contributed to measurements in high magnetic fields. All co-authors reviewed the data analysis and manuscript.

FUNDING

This work was performed at the National High Magnetic Field Laboratory, which is supported by National Science Foundation Cooperative Agreement No. DMR-1644779 and the State of Florida. Synthesis of crystalline materials and their characterization were supported by the Center for Actinide Science and Technology (CAST), an Energy Frontier Research Center (EFRC) funded by the US. Department of Energy (DOE), Office of Science, Basic Energy Sciences (BES), under Award No. DE-SC0016568.

SUPPLEMENTARY MATERIAL

The Supplementary Material for this article can be found online at: https://www.frontiersin.org/articles/10.3389/femat.2022.861448/full#supplementary-material

REFERENCES

Amitsuka, H., Hyomi, K., Nishioka, T., Miyako, Y., and Suzuki, T. (1988). Specific Heat and Susceptibility of U(Ru1−xRhx)2Si2. *J. Magnetism Magn. Mater.* 76-77, 168–170. doi:10.1016/0304-8853(88)90354-x

Bareille, C., Boariu, F. L., Schwab, H., Lejay, P., Reinert, F., and Santander-Syro, A. F. (2014). Momentum-resolved Hidden-Order gap Reveals Symmetry Breaking and Origin of Entropy Loss in URu2Si2. *Nat. Commun.* 5, 4326. doi:10.1038/ncomms5326

Bauer, E. D., Zapf, V. S., Ho, P.-C., Butch, N. P., Freeman, E. J., Sirvent, C., et al. (2005). Non-Fermi-Liquid Behavior within the Ferromagnetic Phase in $URu_{2-x}Re_xSi_2$. *Phys. Rev. Lett.* 94, 046401. doi:10.1103/physrevlett.94.046401

Baumbach, R. E., Fisk, Z., Ronning, F., Movshovich, R., Thompson, J. D., and Bauer, E. D. (2014). High Purity Specimens of URu2Si2produced by a Molten Metal Flux Technique. *Philos. Mag.* 94, 3663–3671. doi:10.1080/14786435.2014.895876

Butch, N. P., Jeffries, J. R., Chi, S., Leão, J. B., Lynn, J. W., and Maple, M. B. (2010). Antiferromagnetic Critical Pressure in URu_2Si_2 under Hydrostatic Conditions. *Phys. Rev. B* 82, 060408. doi:10.1103/physrevb.82.060408

Butch, N. P., and Maple, M. B. (2009). Evolution of Critical Scaling Behavior Near a Ferromagnetic Quantum Phase Transition. *Phys. Rev. Lett.* 103, 076404. doi:10.1103/physrevlett.103.076404

Butch, N. P., and Maple, M. B. (2010). The Suppression of Hidden Order and the Onset of Ferromagnetism in URu2Si2via Re Substitution. *J. Phys. Condens. Matter* 22, 164204. doi:10.1088/0953-8984/22/16/164204

Chappell, G. L., Gallagher, A., Graf, D. E., Riseborough, P., and Baumbach, R. E. (2020). Influence of Hydrostatic Pressure on Hidden Order, the Kondo Lattice, and Magnetism in URu2Si2−xPx. *Phys. Rev. B* 102, 245152. doi:10.1103/physrevb.102.245152

Dalichaouch, Y., Maple, M. B., Chen, J. W., Kohara, T., Rossel, C., Torikachvili, M. S., et al. (1990a). Effect of Transition-Metal Substitutions on Competing Electronic Transitions in the Heavy-Electron compoundURu2Si2. *Phys. Rev. B* 41, 1829–1836. doi:10.1103/physrevb.41.1829

Dalichaouch, Y., Maple, M. B., Guertin, R. P., Kuric, M. V., Torikachvili, M. S., and Giorgi, A. L. (1990b). Ferromagnetism and Heavy Electron Behavior in URu2−xMxSi2(M = Re, Tc and Mn). *Physica B: Condensed Matter* 163, 113–116. doi:10.1016/0921-4526(90)90141-g

Dalichaouch, Y., Maple, M. B., Torikachvili, M. S., and Giorgi, A. L. (1989). Ferromagnetic Instability in the Heavy-Electron compoundURu2Si2doped with Re or Tc. *Phys. Rev. B* 39, 2423–2431. doi:10.1103/physrevb.39.2423

Das, P., Kanchanavatee, N., Helton, J. S., Huang, K., Baumbach, R. E., Bauer, E. D., et al. (2015). Chemical Pressure Tuning of URu_2Si_2 via Isoelectronic Substitution of Ru with Fe. *Phys. Rev. B* 91, 085122. doi:10.1103/physrevb.91.085122

De Boer, F. R., Franse, J. J. M., Louis, E., Menovsky, A. A., Mydosh, J. A., Palstra, T. T. M., et al. (1986). High-magnetic-field and High-Pressure Effects in Monocrystalline URu2Si2. *Physica B+C* 138, 1–6. doi:10.1016/0378-4363(86)90486-9

Endstra, T., Nieuwenhuys, G. J., and Mydosh, J. A. (1993). Hybridization Model for the Magnetic-Ordering Behavior of Uranium- and Cerium-Based 1:2:2 Intermetallic Compounds. *Phys. Rev. B* 48, 9595–9605. doi:10.1103/physrevb.48.9595

Gallagher, A., Chen, K.-W., Moir, C. M., Cary, S. K., Kametani, F., Kikugawa, N., et al. (2016a). Unfolding the Physics of URu2Si2 through Silicon to Phosphorus Substitution. *Nat. Commun.* 7, 10712. doi:10.1038/ncomms10712

Gallagher, A., Chen, K.-W., Cary, S. K., Kametani, F., Graf, D., Albrecht-Schmitt, T. E., et al. (2016b). Thermodynamic and Electrical Transport Investigation of URu2Si2−xPx. *J. Phys. Condens. Matter* 29, 024004. doi:10.1088/0953-8984/29/2/024004

Hassinger, E., Knebel, G., Izawa, K., Lejay, P., Salce, B., and Flouquet, J. (2008). Temperature-pressure Phase Diagram ofURu2Si2from Resistivity Measurements and Ac Calorimetry: Hidden Order and Fermi-Surface Nesting. *Phys. Rev. B* 77, 115117. doi:10.1103/physrevb.77.115117

Huang, K., Chen, K.-W., Gallagher, A., Lai, Y., Nelson, L., Graf, D., et al. (2019). Instability of the F -electron State in URu2Si2−xPx Probed Using High Magnetic fields. *Phys. Rev. B* 99, 235146. doi:10.1103/physrevb.99.235146

Jeffries, J. R., Butch, N. P., Yukich, B. T., and Maple, M. B. (2007). Competing Ordered Phases inURu2Si2: Hydrostatic Pressure and Rhenium Substitution. *Phys. Rev. Lett.* 99, 217207. doi:10.1103/physrevlett.99.217207

Jeffries, J. R., Butch, N. P., Yukich, B. T., and Maple, M. B. (2008). The Evolution of the Ordered States of Single-crystal URu2Si2under Pressure. *J. Phys. Condens. Matter* 20, 095225. doi:10.1088/0953-8984/20/9/095225

Kanchanavatee, N., Janoschek, M., Baumbach, R. E., Hamlin, J. J., Zocco, D. A., Huang, K., et al. (2011). Twofold Enhancement of the Hidden-Order/large-Moment Antiferromagnetic Phase Boundary in the URu2−xFexSi2system. *Phys. Rev. B* 84, 245122. doi:10.1103/physrevb.84.245122

Kanchanavatee, N., White, B. D., Burnett, V. W., and Maple, M. B. (2014). Enhancement of the Hidden Order/large Moment Antiferromagnetic Transition Temperature in the URu2−xOsxSi2system. *Philos. Mag.* 94, 3681–3690. doi:10.1080/14786435.2014.886022

Kawarazaki, S., Kobashi, Y., Taniguchi, T., Miyako, Y., and Amitsuka, H. (1994). Frozen-In Devil's Staircase in U(Ru1-xRhx)2Si2Mixed Compound System as Studied by Neutron Diffraction. *J. Phys. Soc. Jpn.* 63, 716–725. doi:10.1143/jpsj.63.716

Kim, K. H., Harrison, N., Jaime, M., Boebinger, G. S., and Mydosh, J. A. (2003a). Magnetic-Field-Induced Quantum Critical Point and Competing Order Parameters inURu2Si2. *Phys. Rev. Lett.* 91, 256401. doi:10.1103/physrevlett.91.256401

Kim, K. H., Harrison, N., Jaime, M., Boebinger, G. S., and Mydosh, J. A. (2003b). Publisher's Note: Magnetic-Field-Induced Quantum Critical Point and Competing Order Parameters inURu2Si2[Phys. Rev. Lett.91, 256401 (2003)]. *Phys. Rev. Lett.* 91, 269902. doi:10.1103/physrevlett.91.269902

Kuwahara, K., Yoshii, S., Nojiri, H., Aoki, D., Knafo, W., Duc, F., et al. (2013). Magnetic Structure of Phase II inU(Ru0.96Rh0.04)2Si2Determined by Neutron Diffraction under Pulsed High Magnetic Fields. *Phys. Rev. Lett.* 110, 216406. doi:10.1103/physrevlett.110.216406

Lee, J., Matsuda, M., Mydosh, J. A., Zaliznyak, I., Kolesnikov, A. I., Süllow, S., et al. (2018). Dual Nature of Magnetism in a Uranium Heavy-Fermion System. *Phys. Rev. Lett.* 121, 057201. doi:10.1103/physrevlett.121.057201

Lee, J., Prokeš, K., Park, S., Zaliznyak, I., Dissanayake, S., Matsuda, M., et al. (2020). Charge Density Wave with Anomalous Temperature Dependence in $UPt_2 Si_2$. *Phys. Rev. B* 102, 041112. doi:10.1103/physrevb.102.041112

Luo, H., Klimczuk, T., Müchler, L., Schoop, L., Hirai, D., Fuccillo, M. K., et al. (2013). Superconductivity in the Cu(Ir1−xPtx)2Se4spinel. *Phys. Rev. B* 87, 214510. doi:10.1103/physrevb.87.214510

Maple, M. B., Chen, J. W., Dalichaouch, Y., Kohara, T., Rossel, C., Torikachvili, M. S., et al. (1986). Partially Gapped Fermi Surface in the Heavy-Electron superconductorURu2Si2. *Phys. Rev. Lett.* 56, 185–188. doi:10.1103/physrevlett.56.185

McElfresh, M. W., Thompson, J. D., Willis, J. O., Maple, M. B., Kohara, T., and Torikachvili, M. S. (1987). Effect of Pressure on Competing Electronic Correlations in the Heavy-Electron systemURu2Si2. *Phys. Rev. B* 35, 43–47. doi:10.1103/physrevb.35.43

Meng, J.-Q., Oppeneer, P. M., Mydosh, J. A., Riseborough, P. S., Gofryk, K., Joyce, J. J., et al. (2013). Imaging the Three-Dimensional Fermi-Surface Pairing Near the Hidden-Order Transition inURu2Si2Using Angle-Resolved Photoemission Spectroscopy. *Phys. Rev. Lett.* 111, 127002. doi:10.1103/physrevlett.111.127002

Miyako, Y., Kawarazaki, S., Amitsuka, H., Paulsen, C. C., and Hasselbach, K. (1991). Magnetic Properties of U(Ru1−xRhx)2Si2single Crystals (0≤x≤1). *J. Appl. Phys.* 70, 5791–5793. doi:10.1063/1.350162

Motoyama, G., Nishioka, T., and Sato, N. K. (2003). Phase Transition between Hidden and Antiferromagnetic Order inURu2Si2. *Phys. Rev. Lett.* 90, 166402. doi:10.1103/physrevlett.90.166402

Motoyama, G., Yokoyama, N., Sumiyama, A., and Oda, Y. (2008). Electrical Resistivity and Thermal Expansion Measurements of URu2Si2 under Pressure. *J. Phys. Soc. Jpn.* 77, 123710. doi:10.1143/jpsj.77.123710

Nieuwenhuys, G. J. (1987). Crystalline Electric Field Effects inUPt2Si2andURu2Si2. *Phys. Rev. B* 35, 5260–5263. doi:10.1103/physrevb.35.5260

Niklowitz, P. G., Pfleiderer, C., Keller, T., Vojta, M., Huang, Y.-K., and Mydosh, J. A. (2010). Parasitic Small-Moment Antiferromagnetism and Nonlinear Coupling of Hidden Order and Antiferromagnetism inURu2Si2Observed by Larmor Diffraction. *Phys. Rev. Lett.* 104, 106406. doi:10.1103/physrevlett.104.106406

Palstra, T. T. M., Menovsky, A. A., Berg, J. v. d., Dirkmaat, A. J., Kes, P. H., Nieuwenhuys, G. J., et al. (1985). Superconducting and Magnetic Transitions in the Heavy-Fermion System URu2Si2. *Phys. Rev. Lett.* 55, 2727–2730. doi:10.1103/physrevlett.55.2727

Palstra, T. T. M., Menovsky, A. A., and Mydosh, J. A. (1986). Anisotropic Electrical Resistivity of the Magnetic Heavy-Fermion superconductorURu2Si2. *Phys. Rev. B* 33, 6527–6530. doi:10.1103/physrevb.33.6527

Ptasiewicz-Bąk, H., Leciejewicz, J., and Zygmunt, A. (1985). *Solid State Communications*, 55. Pergamon Press, 601.

Rahn, M. C., Gallagher, A., Orlandi, F., Khalyavin, D. D., Hoffmann, C., Manuel, P., et al. (2021). Collinear Antiferromagnetic Order in URu2Si2−xPx Revealed by Neutron Diffraction. *Phys. Rev. B* 103, 214403. doi:10.1103/physrevb.103.214403

Ran, S., Wolowiec, C. T., Jeon, I., Pouse, N., Kanchanavatee, N., White, B. D., et al. (2016). Phase Diagram and thermal Expansion Measurements on the System URu 2− X Fe X Si 2. *Proc. Natl. Acad. Sci. U.S.A.* 113, 13348–13353. doi:10.1073/pnas.1616542113

Santander-Syro, A. F., Klein, M., Boariu, F. L., Nuber, A., Lejay, P., and Reinert, F. (2009). Fermi-surface Instability at the 'hidden-Order' Transition of URu2Si2. *Nat. Phys* 5, 637–641. doi:10.1038/nphys1361

Schlabitz, W., Baumann, J., Pollit, B., Rauchschwalbe, U., Mayer, H. M., Ahlheim, U., et al. (1986). Superconductivity and Magnetic Order in a Strongly Interacting Fermi-System: URu2Si2. *Z. Physik B - Condensed Matter* 62, 171–177. doi:10.1007/bf01323427

Szytuka, A., Siek, S., Leciejewicz, J., Zygmunt, A., and Ban, Z. (1988). Neutron Diffraction Study of UT2X2 (T = Mn, Fe, X = Si, Ge) Intermetallic Systems. *J. Phys. Chem. Sol.* 49, 1113–1118. doi:10.1016/0022-3697(88)90162-x

Umarji, A. M., Yakhmi, J. V., Tomy, C. V., Iyer, R. M., Gupta, L. C., and Vijayaraghavan, R. (1987). "Resistivity Studies on UM2Si2 (M = Rh, Ir, Ru and Os)," in *Theoretical and Experimental Aspects of Valence Fluctuations and Heavy Fermions*. Editors L. C. Gupta and S. K. Malik (Boston, MA: Springer US), 341–344. doi:10.1007/978-1-4613-0947-5_39

Wartenbe, M. R., Chen, K.-W., Gallagher, A., Harrison, N., McDonald, R. D., Boebinger, G. S., et al. (2017). Role of Band Filling in Tuning the High-Field Phases of $URu_2 Si_2$. *Phys. Rev. B* 96, 085141. doi:10.1103/physrevb.96.085141

Wiebe, C. R., Janik, J. A., MacDougall, G. J., Luke, G. M., Garrett, J. D., Zhou, H. D., et al. (2007). Gapped Itinerant Spin Excitations Account for Missing Entropy in the Hidden-Order State of URu2Si2. *Nat. Phys* 3, 96–99. doi:10.1038/nphys522

Wilson, M. N., Williams, T. J., Cai, Y.-P., Hallas, A. M., Medina, T., Munsie, T. J., et al. (2016). Antiferromagnetism and Hidden Order in Isoelectronic Doping of $URu_2 Si_2$. *Phys. Rev. B* 93, 064402. doi:10.1103/physrevb.93.064402

Yokoyama, M., and Amitsuka, H. (2007). Evolution of Heterogeneous Antiferromagnetic State in URu2Si2: Study of Hydrostatic-Pressure, Uniaxial-Stress and Rh-Dope Effects. *J. Phys. Soc. Jpn.* 76, 136–139. doi:10.1143/jpsjs.76sa.136

Yokoyama, M., Amitsuka, H., Itoh, S., Kawasaki, I., Tenya, K., and Yoshizawa, H. (2004). Neutron Scattering Study on Competition between Hidden Order and Antiferromagnetism in U(Ru1-xRhx)2Si2(x≤0.05). *J. Phys. Soc. Jpn.* 73, 545–548. doi:10.1143/jpsj.73.545

Yoshida, R., Nakamura, Y., Fukui, M., Haga, Y., Yamamoto, E., Ōnuki, Y., et al. (2010). Signature of Hidden Order and Evidence for Periodicity Modification inURu2Si2. *Phys. Rev. B* 82, 205108. doi:10.1103/physrevb.82.205108

Zhu, X., Han, F., Mu, G., Cheng, P., Tang, J., Ju, J., et al. (2010). Superconductivity Induced by Doping Platinum inBaFe2As2. *Phys. Rev. B* 81, 104525. doi:10.1103/physrevb.81.104525

Żołnierek, Z., and Mulak, J. (1995). *Journal of Magnetism and Magnetic Materials*, 1393, 140–144. North-Holland Publishing Company. international Conference on Magnetism.

Conflict of Interest: The authors declare that the research was conducted in the absence of any commercial or financial relationships that could be construed as a potential conflict of interest.

Publisher's Note: All claims expressed in this article are solely those of the authors and do not necessarily represent those of their affiliated organizations, or those of the publisher, the editors and the reviewers. Any product that may be evaluated in this article, or claim that may be made by its manufacturer, is not guaranteed or endorsed by the publisher.